

## Statistical aspects of a quantum Hopfield model

Shuohang Wu<sup>1</sup> and Zi Cai<sup>1,2,\*</sup>

<sup>1</sup>*Wilczek Quantum Center and Key Laboratory of Artificial Structures and Quantum Control, School of Physics and Astronomy, Shanghai Jiao Tong University, Shanghai 200240, China*

<sup>2</sup>*Shanghai Research Center for Quantum Sciences, Shanghai 201315, China*



(Received 7 May 2022; revised 29 April 2023; accepted 15 May 2023; published 24 May 2023)

In this paper, we study the eigenstate properties of a quantum Hopfield model by the exact diagonalization method. The local permutational symmetry in this model organizes the spins into clusters, which can each be considered a large quantum spin interacting with others. It is shown that such a quantum Hopfield model, even though without dissipation, is interesting in its own right as an example of quantum frustrated magnetism and quantum spin glass. It exhibits three distinct phases: a low-energy spin-glass phase at a low transverse field, a thermal paramagnetic phase at a high transverse field, and a nonthermal high-energy paramagnetic phase. The dynamics of the revival probability starting from a memory pattern in such a closed quantum many-body model has also been studied.

DOI: [10.1103/PhysRevB.107.184310](https://doi.org/10.1103/PhysRevB.107.184310)

### I. INTRODUCTION

Human memory is one of the most prominent emergent phenomena in neural networks, where memory patterns are retrieved by association. A toy model, known as the Hopfield model, is proposed to illustrate the associative memory from the perspective of statistical physics [1]. In such a classical statistical model, the emergent dynamically stable configurations are correlated with certain memory patterns, which enables the system to retrieve the correct stored configuration via the classical annealing process [2,3]. From the statistical physics point of view, the Hopfield model is one type of spin-glass (SG) model [4], while the strong disorder correlation between the bonds in the Hopfield model yields a structure considerably simpler [5] than that in conventional SG models [6,7]. Although the SG is essentially classical, incorporating the quantum effect gives rise to a plethora of novel phenomena due to the interplay between quantum fluctuations and the frustration-induced rugged energy landscape [8–12]. To realize a quantum generalization of the retrieval phase of the classical Hopfield model, one needs to include dissipation into the quantum Hopfield model to mimic classical annealing [13,14]. However, as we will show in the following, the closed quantum Hopfield model without dissipation, as an example of frustrated quantum magnetism and quantum SG, is interesting in its own right. Some analytic progress has been made for this quantum Hopfield model, including the revelation of independent free energy from the choices of patterns in the case  $p \leq \alpha N$  with  $\alpha \neq 0$  and  $N \rightarrow \infty$  [15].

In this paper, we consider the quantum Hopfield model as a closed quantum many-body system and investigate its eigenstate properties using exact diagonalization (ED). The local permutation symmetry of this model enables us to

explore systems with relatively large system size. It is shown that according to the strength of quantum fluctuation (transverse field) and the energy, the eigenstates of this model can be classified into three distinct groups: The low-energy eigenstates with weak transverse field are characterized by SG ordering with spontaneous  $Z_2$  symmetry breaking, while in the presence of strong transverse field, the quantum SG phase gives way to a thermal paramagnetic (PM) phase. Most interestingly, the high-energy eigenstates at weak transverse field seem to be also paramagnetic but nonthermal, which is characterized by the absence of energy repulsion in the level space statistics. The quantum dynamics starting from particular spin configurations (memory patterns) has also been investigated to characterize the revival probability in such a closed system.

### II. MODEL AND METHOD

The studied model is a quantum generalization of the Hopfield model whose Hamiltonian is a transverse Ising model with all-to-all coupling:

$$H = -\frac{1}{2} \sum_{i \neq j} J_{ij} \hat{s}_i^z \hat{s}_j^z - h_x \sum_i \hat{s}_i^x, \quad (1)$$

where  $\hat{s}_i^\alpha = \frac{1}{2} \hat{\sigma}_i^\alpha$ , with  $\alpha = x, y, z$  and  $\hat{\sigma}_i^\alpha$  being Pauli matrices on site  $i$ , and  $h_x$  is the strength of the uniform transverse magnetic field. The interaction strength between sites  $i$  and  $j$  is defined as

$$J_{ij} = \frac{J}{N} \sum_{\mu=1}^p \xi_i^\mu \xi_j^\mu, \quad (2)$$

where  $N$  is the number of lattice sites.  $p$  is the number of patterns embedded in the system ( $\mu$  is the pattern index), where each pattern can be considered as an  $N$ -dimensional vector  $\vec{\xi}^\mu = \{\xi_1^\mu, \xi_2^\mu, \dots, \xi_N^\mu\}$  with  $\xi_i^\mu$  taken to be quenched,

\*zcai@sjtu.edu.cn

independent, random variables ( $\xi_i^\mu = \pm 1$  with equal probabilities). Memory patterns  $\tilde{\xi}^\mu$  are stored in the quenched random couplings via Eq. (2).

In the absence of the transverse field ( $h_x = 0$ ), the Hamiltonian (1) is reduced to a classical Hopfield model with the capacity to retrieve information embedded in the memory patterns  $\tilde{\xi}^\mu$ . If one begins from a classical spin configuration similar enough to one of the stored patterns  $\tilde{\xi}^\mu$ , the classical Hopfield model system could retrieve the correct pattern via classical annealing. In the thermodynamic limit ( $N \rightarrow \infty$ ), such a retrieval occurs if  $p/N$  is less than a critical value [2], whereas for cases with a finite  $p$ , the energy of the classical Hamiltonian is minimized by the  $2p$  spin configurations:  $\vec{s} = \pm \frac{1}{2} \tilde{\xi}^{1 \dots p}$  (Mattis states). The symmetric and asymmetric mixing of these Mattis states as metastable states has also been analyzed [3].

Now, we turn to the quantum Hamiltonian (1) ( $h_x > 0$ ), where we choose the basis as the eigenstates of  $\hat{s}^z$ :  $|\vec{s}\rangle = |s_1^z, \dots, s_N^z\rangle$ . The analysis in this paper is restricted to the case of a small finite  $p$ . We first analyze the symmetry of Eq. (1). The simplest case is  $p = 1$ , where the disorder can be gauged away [16] and there is no frustration. By performing a gauge transformation,

$$\tilde{s}_i^z = \xi_i^1 \hat{s}_i^z, \quad (3)$$

the Hamiltonian (1) becomes a ferromagnetic (FM) transverse Ising model with uniform all-to-all coupling, where the *permutational symmetry* (PS) among different sites allows us to combine all the spins into a combined spin with operators  $\hat{S}^\alpha = \sum_i \tilde{s}_i^\alpha$  and Eq. (1) becomes a Lipkin-Meshkov-Glick (LMG) Hamiltonian [17],

$$H_1 = -\frac{J}{2N} (\hat{S}^z)^2 - h_x \hat{S}^x, \quad (4)$$

with the self-interaction term  $i = j$  included, which is just a constant term. Such a gauge transformation applies not only for  $p = 1$ , but also for general  $p$  cases, where we can always choose one of the patterns (say, pattern 1), and transform it into an FM pattern via the transformation in Eq. (3); all the other patterns are also changed accordingly as

$$\tilde{\xi}_i^\mu = \xi_i^1 \xi_i^\mu, \quad (5)$$

and thus the original memory patterns  $\{\tilde{\xi}^\mu\}$  have been transformed into a set of new ones  $\{\tilde{\xi}^\mu\}$ , where at least one of them is a uniform FM pattern satisfying  $\xi_i^1 = 1 \forall i$ . Therefore, without losing generality, in the following discussion, we always choose pattern 1 as the FM pattern.

For  $p = 2$ , the system can be divided into two clusters according to the sign of  $\xi_i^1 \xi_i^2$ : The  $i$ th site satisfying  $\xi_i^1 \xi_i^2 = 1$  ( $-1$ ) belongs to cluster 1 (2). Similar to  $p = 1$ , the PS within each cluster enables us to combine the spins within it as  $\hat{S}_a^\alpha = \sum_{i \in a} \hat{s}_i^\alpha$ , where  $a = 1, 2$  is the cluster index. It is easy to check that there is no coupling between the two clusters according to Eq. (2), and the Hamiltonian turns into two decoupled LMG models, as shown in Fig. 1(b). For the cases with  $p > 2$ , the lattice sites can be classified into  $2^{p-1}$  clusters, each of which is a combined spin interacting with others via the FM or antiferromagnetic (AFM) coupling. For example, the classification scheme of lattice sites for  $p = 3$  is shown

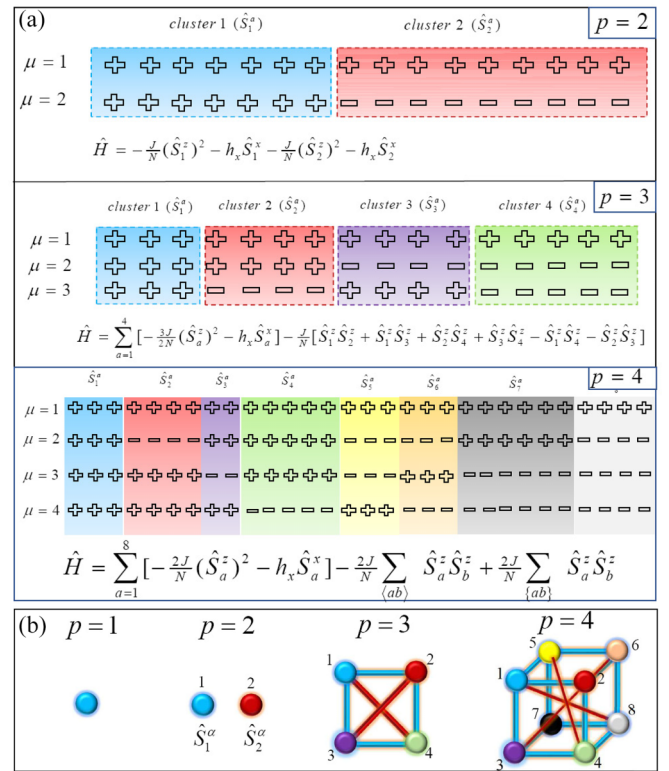


FIG. 1. (a) Classification scheme of lattice sites and effective Hamiltonian for  $p = 2$ ,  $p = 3$ , and  $p = 4$ .  $\mu$  is the index of patterns. (b) Sketches of the effective Hamiltonian for  $p = 1-4$ , where the combined spins are located on the vertex and the blue (red) bonds represent FM (AFM) couplings between them.

in Fig. 1(a), where each cluster is represented by a combined spin located on the vertex of a square. The blue bonds denote FM interactions, and the red ones represent AFM couplings, which lead to frustration. Similarly, for  $p = 4$ , the Hamiltonian of the quantum Hopfield model can be expressed in terms of the combined spin operators as

$$H = \sum_{a=1}^8 \left[ -\frac{2J}{N} (\hat{S}_a^z)^2 - h_x \hat{S}_a^x \right] - \frac{2J}{N} \sum_{\langle ab \rangle} \hat{S}_a^z \hat{S}_b^z + \frac{2J}{N} \sum_{\{ab\}} \hat{S}_a^z \hat{S}_b^z, \quad (6)$$

where  $\hat{S}_a^{z/x} = \sum_{i \in a} \hat{s}_i^{z/x}$  is the spin operator of cluster  $a$ ,  $\sum_{\langle ab \rangle}$  is the summation over the bonds on the 12 edges of the cube as shown in Fig. 1(b), which represents ferromagnetic coupling, and  $\sum_{\{ab\}}$  is the summation over the bonds on the four body diagonals of the cube, which represents the antiferromagnetic couplings. It is worth noticing that there is no coupling between the two spins along the surface diagonals of the cube.

In this paper, we study the properties of eigenstates of the Hamiltonian (1) via the exact diagonalization method. The PS within each cluster allows us to block-diagonalize the Hamiltonian. Throughout this paper, we choose the fully symmetric subspace, which corresponds to the Hilbert space with the largest total spin. Accounting for the PS not only significantly reduces the Hilbert space dimension, but also allows us to resolve the accidental degeneracy between the energy levels in subspaces with different conserved quantities, which is important to analyze the level space statistics. In the following,

we focus on the case of  $p = 4$ , which represents a generic situation of the Hopfield model with finite  $p$ , in contrast to the “special” cases (e.g.,  $p = 1, 2$ ). (The  $p = 3$  case has also been checked, and there is no qualitative difference between the cases with  $p = 3$  and  $p = 4$ .)

We randomly sample  $\mathcal{N}$  sets of independent memory patterns  $\{\bar{\xi}^1 \dots \bar{\xi}^p\}$  with  $\mathcal{N} = 10^3$ , and the ensemble average is performed over all  $\mathcal{N}$  pattern realizations. For certain special memory patterns, additional symmetry other than the local permutational symmetry may emerge in the effective Hamiltonian. These additional symmetries could give rise to accidental degeneracy in the energy spectrum. Take the case of  $p = 3$  as an example, where the sites are classified into four clusters as shown in Fig. 1(b), for a special configuration with  $N_i = N/4 \forall i$ , with  $N_i$  being the number of spins in the  $i$ th cluster; the systems become a spin chain with next-nearest interactions and periodic boundary conditions, and thus there is an additional translational (or fourfold rotational) symmetry, which will give rise to conserved quantities that may lead to accidental degeneracy. Even though the probability of these special patterns approaches zero in the thermodynamic limit, they do exist in pattern sampling for finite-size systems and thus will change the properties of the energy level statistics. Therefore we eliminate these kinds of special patterns in our sampling.

### III. SPIN-GLASS TRANSITION

In the classical limit ( $h_x = 0$ ), the system experiences a thermal phase transition from a low-temperature SG-like magnetic phase to a high-temperature paramagnetic phase. In the presence of a weak transverse field, we conjecture that there may be a similar transition that separates the low- and high-energy eigenstates of the Hamiltonian (1). To verify this point numerically, we define the SG susceptibility for the  $n$ th eigenstate  $|n\rangle$  [9,18],

$$\chi_n = \frac{1}{N} \sum_{i,j} \langle n | \hat{s}_i^z \hat{s}_j^z | n \rangle^2, \quad (7)$$

and calculate its dependence on the normalized energy density  $\epsilon = \frac{E_n - E_{\min}}{E_{\max} - E_{\min}}$ , where  $E_n$  is the eigenenergy of  $|n\rangle$  and  $E_{\min}$  ( $E_{\max}$ ) is the minimum (maximum) eigenenergy. We define  $\chi(\epsilon) = \langle \chi_n \rangle_\epsilon$ , where the average  $\langle \rangle_\epsilon$  is performed over all the eigenstates within the energy window  $[\epsilon, \epsilon + \Delta]$  with  $\Delta = 0.01$ . We plot  $\chi(\epsilon)$  with a small fixed transverse field ( $h_x = 0.1J$ ) for various system sizes in Fig. 2(a), which shows that at low energy,  $\chi(\epsilon)$  linearly diverges with the system size [ $\chi(\epsilon) \sim N$ ]: a signature of spin freezing and long-range correlation. In contrast, at high energy,  $\chi(\epsilon)$  approaches a finite value in the thermodynamic limit, indicating a short-range correlation only. The distinct behaviors of  $\chi(\epsilon)$  between the low- and high-energy eigenstates suggest a phase transition between them, which is characterized by the crossing point ( $\epsilon_c$ ) between the  $\chi(\epsilon)$  curves with different  $N$ .

Generally, quantum fluctuation also suppresses the SG order in the low-energy eigenstates and makes it give way to a quantum paramagnetic phase, which is similar to what happens in a conventional transverse Ising model. To verify this point, we restrict our discussion for the ground state of

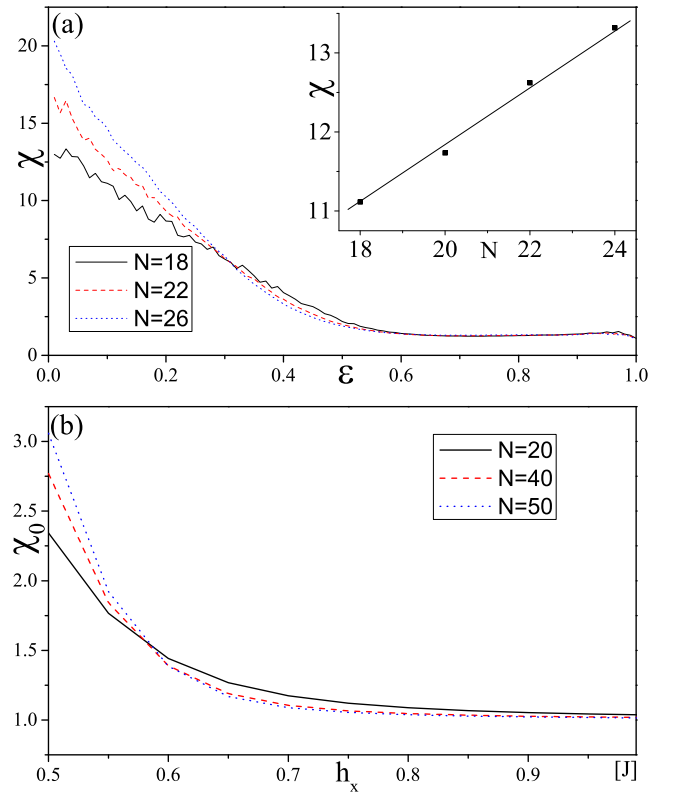


FIG. 2. (a) Spin-glass susceptibility  $\chi$  as a function of normalized energy  $\epsilon$  for different system sizes with  $h_x = 0.1J$ . The inset indicates the system size dependence of  $\chi$  with a fixed  $\epsilon = 0.1$  within the SG phase. (b) Spin-glass susceptibility  $\chi_0$  of the ground state as a function of transverse field  $h_x$  for different system sizes.

the Hamiltonian (1) and tune the strength of the transverse field  $h_x$ . We also use the corresponding SG susceptibility  $\chi_0$  [ $n = 0$  in Eq. (7) corresponds to the ground state  $|0\rangle$ ] to characterize the quantum phase transition induced by quantum fluctuations. The ground state can be obtained by the Lanczos algorithm, which enables us to diagonalize systems with relatively larger system size (up to  $N = 50$ ). The dependence of  $\chi_0$  on  $h_x$  is plotted in Fig. 2(b), which also exhibits a crossing point at a critical transverse field  $h_c \simeq 0.57J$  for the curves of different system sizes. Below this critical point,  $\chi_0$  diverges with the system size, indicating the presence of SG long-range order. For  $h_x > h_c$ ,  $\chi_0$  extrapolates a finite value that is independent of  $N$ , which is similar to the high-energy case studied above.

In summary, the low-energy eigenstates of the Hamiltonian (1) with weak transverse field are in a SG phase, which can be destroyed by either increasing the energy or increasing the transverse field. In spite of the similarity between the PM phase driven by the energy and that driven by the transverse field, an important question is whether they belong to the same class. In a quantum  $p$ -spin model, there exists an intermediate nonthermal PM phase at a small transverse field, which is different from a thermal PM phase at a large transverse field [8], whereas numerical studies of a quantum Sherrington and Kirkpatrick model seem to suggest a different scenario [9]. In the following, we will show that there indeed

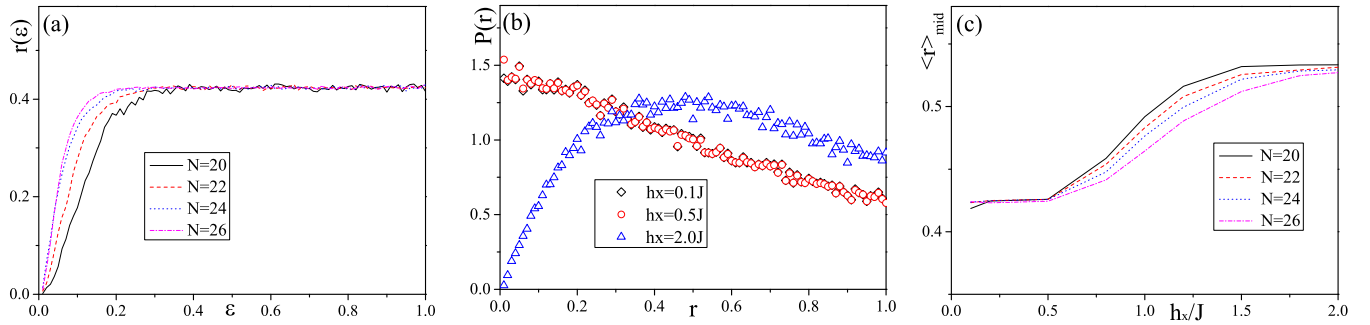


FIG. 3. (a) Average ratio of adjacent level spacing  $r(\epsilon)$  as a function of normalized energy  $\epsilon$  with different system sizes and fixed  $h_x = 0.1J$ . (b) Distributions of  $r_n$  in the thermal ( $h_x = 2J$ ) and nonthermal ( $h_x = 0.1J$ ) paramagnetic eigenstates. (c) Dependence of the average  $r_n$  on  $h_x$  in the paramagnetic phases. The statistics and average are performed over the eigenstates within the normalized energy window  $\epsilon \in [0.45, 0.55]$  for (b) and (c).

exist two different PM phases in the quantum Hopfield model, while neither of them is a many-body localized (MBL) phase.

#### IV. A LEVEL SPACE STATISTICS DIAGNOSIS

The thermal PM phase at a large transverse field can be distinguished from the nonthermal PM phase with high energy but small transverse field via the energy level repulsion, which in turn can be determined by the ratio of adjacent level spacing in the energy spectrum  $r_n = \frac{\min(\delta_n, \delta_{n+1})}{\max(\delta_n, \delta_{n+1})}$  [19], where  $\delta_n = E_n - E_{n-1}$  is the level spacing between consecutive energy levels in the ordered list of eigenenergies  $\{E_n\}$  of the Hamiltonian. For thermal states, the distribution of the level spacing  $P(r)$  is expected to follow a Gaussian orthogonal ensemble (GOE) [20], which is characterized by the vanishing of  $P(r)$  for  $r \rightarrow 0$  (level repulsion) and a mean value  $\langle r_n \rangle \simeq 0.536$ , while for nonthermal phases,  $P(r)$  typically follows a Poisson distribution with a mean value  $\langle r_n \rangle \simeq 0.386$ .

We first focus on the case with a weak transverse field and study the  $\epsilon$  dependence of  $r(\epsilon) = \langle r_n \rangle_\epsilon$  with a fixed  $h_x = 0.1J$ . As shown in Fig. 3(a), for small  $\epsilon$ ,  $r(\epsilon)$  strongly depends on the system size, and its values are significantly smaller than the average values in the GOE or Poisson distributions. This is because at low energy, an SG phase is accompanied by a spontaneous  $Z_2$  symmetry breaking. The typical gap between a low-energy eigenstate and its  $Z_2$  symmetric counterpart is exponentially small; thus the average value of  $r_n$  is lowered [21]. For large  $\epsilon$ ,  $r(\epsilon)$  approaches the value of 0.41, slightly higher than the mean value of Poisson distributions. To explore the properties of the high-energy eigenstates, we focus on the eigenstates within energy windows around the spectrum center ( $\epsilon_n \in [0.45, 0.55]$ ) and calculate their  $r_n$  distribution, which resembles the Poisson distribution but is far from the GOE distribution, as shown in Fig. 3(b).

One may wonder whether the absence of level repulsion in the case of small  $h_x$  is due to some trivial reasons, for instance, a “hidden” symmetry other than PS that can be used to further block-diagonalize the Hamiltonian and thus give rise to accidental degeneracy between the energy levels in different blocks. To preclude this possibility, we study the case with a large  $h_x$ , whose Hamiltonian shares exactly the same symmetries with the small- $h_x$  ones. Figure 3(b) shows that the distribution of  $r_n$  in the case of  $h_x = 2J$  follows the GOE statistics, indicating that there are two types of PM states:

the thermal eigenstates of the Hamiltonian (1) with large  $h_x$  and the nonthermal ones in the small- $h_x$  cases. The difference between them can be characterized by  $\langle r_n \rangle_{\text{mid}}$ , where the average  $\langle \rangle_{\text{mid}}$  is over eigenstates within energy windows around the spectrum center ( $\epsilon_n \in [0.45, 0.55]$ ). The dependence of  $\langle r_n \rangle_{\text{mid}}$  on  $h_x$  for different system sizes is plotted in Fig. 3(c), which seems to indicate a crossover instead of a phase transition between the two PM phases.

Another possible trivial explanation for the absence of level repulsion is that the value of  $h_x$  we choose ( $h_x = 0.1J$ ) is too small and thus the thermalization can only be seen in a relatively large system which is beyond the largest system size in our current simulation. It is known that for an integrable model with a small integrability-breaking perturbation, even though the system is known to be thermalized by the perturbation in the thermodynamic limit, for a finite (small) system, the  $P(r)$  still looks similar to the Poisson distribution. The GOE statistics can only be seen in a sufficiently large system [22–25]. In addition, for some models with small perturbation, it is possible that new conserved quantities could emerge in the corresponding effective model (e.g., an emergent global conservation law of the domain wall number in a  $d$ -dimensional transverse Ising model [26]). To preclude the possibility that the absence of level repulsion is an artifact of small  $h_x$ , we calculate  $P(r)$  for the case with a relatively large  $h_x$ . As shown in Fig. 3(b), there is no qualitative difference between the  $P(r)$  in the case with  $h_x = 0.1J$  and that in the case with  $h_x = 0.5J$  (notice that the ground-state quantum phase transition occurs at  $h_c = 0.56J$  and thus  $h_x = 0.5J$  is a relatively large value and already close to the critical point), indicating that the absence of level repulsion is *not* an artifact of the finite-size effect in the presence of small  $h_x$ .

#### V. OTHER PROPERTIES OF THE NONTHERMAL PARAMAGNETIC STATES

Another diagnostic of thermalization for quantum systems is the eigenstate thermalization hypothesis (ETH) [27–29], which states that for a sufficiently large generic quantum many-body system, the expectation value of a few-body operator in an eigenstate of the Hamiltonian is a smooth function of its eigenenergy. To examine the ETH, we choose the operator of the FM order parameter,  $M_n = \frac{1}{N} \sqrt{\langle n | (\sum_i \hat{s}_i^z)^2 | n \rangle}$ , and calculate its expectation value in different eigenstates as a

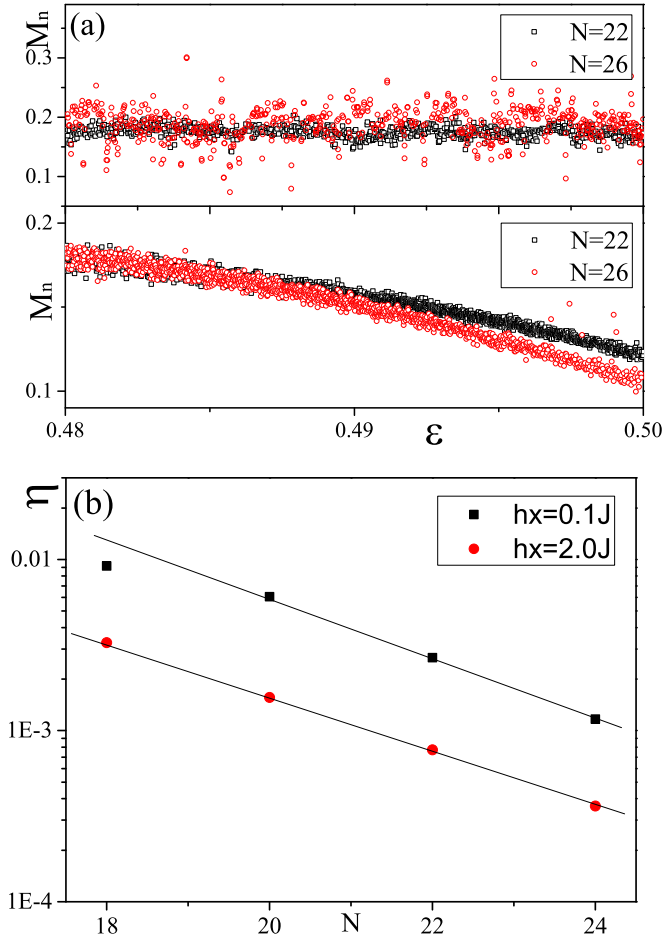


FIG. 4. (a) Eigenstate expectation values of the FM order parameters  $M_n$  as a function of  $\epsilon$  in the nonthermal ( $h_x = 0.1J$ , upper panel) and thermal ( $h_x = 2J$ , lower panel) phases. (b) System size dependence of the averaged partition ratio  $\eta$  for different  $h_x$ , where the statistics and average are performed over the eigenstates within the normalized energy window  $\epsilon \in [0.45, 0.55]$ .

function of eigenenergies. As shown in Fig. 4(a), for a fixed  $\epsilon$  close to the spectrum center, the distribution of  $M_n$  is diverse in the nonthermal PM phase ( $h_x = 0.1J$ ), and its variance increases with the system size, which seems to indicate that the ETH is broken. Persuasive evidence of ETH breaking calls for a systematic comparison between the variances of  $M_n$  for different system sizes. However, due to the large statistical error bar and limited system size in our simulation, it is difficult to conclude whether ETH is broken or not for the high-energy paramagnetic states.

A well-known example of a high-energy nonthermal state is the many-body localized phase [19,30–32], where the physical origin of ergodicity breaking is the quantum-interference effect. To distinguish the nonthermal state in the quantum Hopfield model from the MBL phases, we calculate the participation ratio of the eigenstates  $\eta = \langle \sum_i |\Psi_n(i)|^4 \rangle_{\text{mid}}$ , where  $\Psi_n(i) = \langle n | \bar{s}_i \rangle$  is the coefficient of the  $n$ th eigenstate projected on the  $i$ th Fock basis  $|\bar{s}_i\rangle$  and  $\langle \rangle_{\text{mid}}$  is defined above. Figure 4(b) shows  $\eta$  as a function of system size for two different PM phases, both of which exhibit exponential decays, indicating that there is no localization in the Fock space for

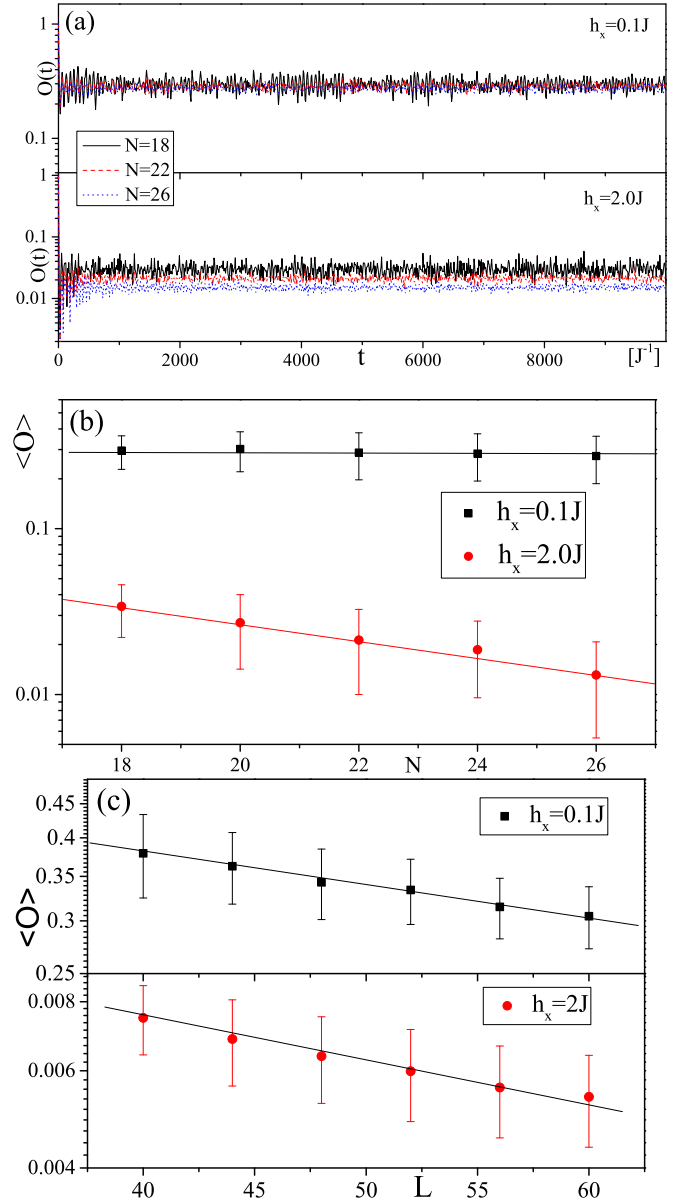


FIG. 5. (a) The time evolution of the revival probability  $O(t)$  for systems with different system sizes and  $h_x = 0.1J$  (upper panel) and  $h_x = 2J$  (lower panel). (b) and (c) The system size dependence of the time-averaged revival probability  $\langle O \rangle$  for  $h_x = 0.1J$  and  $h_x = 2J$  in the model with  $p = 4$  (b) and  $p = 3$  (c).

either thermal or nonthermal PM eigenstates and thus neither of them is an MBL state.

## VI. REVIVAL PROBABILITY OF THE MEMORY PATTERNS

In the classical Hopfield model, it is known that associative memory is related to a classical annealing process, where dissipation is important to drive the system into the memory patterns (stable low-energy configurations). In our closed quantum Hopfield model, there is no dissipation; thus it is an interesting question whether the system can memorize its initial state information. In general, when thermalization occurs,

all the initial state information except energy is washed out after a sufficiently long time, and the system can be described by a statistical ensemble. However, for a nonthermal state, it is possible that the initial state information can be partially preserved.

We choose the initial state as one of  $p$  memory patterns ( $\vec{\xi}^\mu$  with  $\mu \in [1, \dots, p]$ ), which is a product state denoted by  $|\psi_0\rangle = |s_1^z s_2^z \cdots s_N^z\rangle$  with  $s_i^z = \xi_i^\mu \forall i$ . During the time evolution, we calculate the revival probability for the system to return to such an initial state:

$$O(t) = |\langle \psi_0 | e^{-iHt} | \psi_0 \rangle|, \quad (8)$$

where  $H$  is the Hamiltonian of the quantum Hopfield model defined in Eq. (1). The average  $\bar{A}$  is performed over the ensemble average of the  $\mathcal{N}$  sets of memory patterns  $\{\vec{\xi}\}$ . In a thermal phase, the thermalization of the wave function indicates that its projection on a particular basis is  $\sim O(1/\sqrt{\mathcal{V}})$ , where  $\mathcal{V}$  is the Hilbert space of the system that diverges exponentially with the system size ( $\mathcal{V} = 4456, 14\,637$ , and  $43\,296$  for  $N = 18, 22$ , and  $26$ , respectively, where  $\bar{\mathcal{V}}$  indicates the average over  $\mathcal{N}$  sets of memory patterns). This agrees with our numerical results for  $h_x = 2J$ . Figure 5(a) indicates that in the case with  $h_x = 2J$  and finite system sizes  $N$ ,  $O(t)$  will quickly decay to a small value accompanied by fluctuations. One can further perform the average over the second half of the simulation time to derive the saturated value of  $O(t)$ :

$$\langle O \rangle = \frac{2}{T} \int_{\frac{T}{2}}^T dt O(t), \quad (9)$$

where  $T = 10^4 J^{-1}$  is the simulation time. Figure 5(b) shows that for  $h_x = 2J$ ,  $\langle O \rangle$  decays exponentially with  $N$  (for instance,  $\langle O \rangle \sim \frac{1}{\sqrt{\mathcal{V}}}$  indicates that the ratio  $\frac{\langle O(L=26) \rangle}{\langle O(L=18) \rangle} = 0.38$  should roughly agree with  $\sqrt{\frac{\bar{\mathcal{V}}(N=18)}{\bar{\mathcal{V}}(N=26)}} = 0.32$  in the thermal phase with  $h_x = 2J$ ). Although for the case with  $h_x = 0.1J$  the saturated value of  $O(t)$  is much larger than that in the case with  $h_x = 2J$ ,  $\langle O \rangle$  slowly decays with system size. However, the difference between the values of  $\langle O \rangle$  with variant  $N$  is significantly smaller than the statistical error bar. To draw a conclusion, we perform the same analysis on the case  $p = 3$ , which allows us to study a larger system size. As shown in

Fig. 5(c), the saturated value of  $O(t)$  decays exponentially with increasing  $N$  with both  $h_x = 0.1J$  and  $h_x = 2J$ , which indicates that the revival probability will go to zero in the thermodynamic limit in both the spin-glass and paramagnetic phases.

## VII. CONCLUSION AND OUTLOOK

In summary, we have studied the eigenstate properties of the quantum Hopfield Hamiltonian and found two different types of PM states in this model. Future developments will include studies of the real-time evolution of this model from the initial states other than the memory patterns, including the quantum quench and periodically driven dynamics. In general, ergodicity breaking indicates that the system will not equilibrate to a thermal state [33,34], but whether it will approach a nonthermal steady state or exhibit persistent oscillations like the quantum scar [35] or the infinite-range interacting systems [36–38] is an interesting question worthy of further study. Furthermore, imposing a periodic drive on such a model does not necessarily drive the system into an infinite-temperature state and thus may open new possibilities to explore nontrivial dynamics such as discrete time crystals [39–42]. Finally, since the Hopfield model is proposed to mimic associative memory, a fundamental question is the relationship between the associative memory and the ergodicity breaking in this quantum model. However, a mimic of the associative memory calls for dissipation, which has not been considered here. Incorporating dissipation further complicates the system but might give rise to intriguing phenomena due to the interplay between the quantum fluctuation and frustration [13,43].

## ACKNOWLEDGMENTS

This work is supported by the National Key Research and Development Program of China (Grant No. 2020YFA0309000), the Natural Science Foundation of China (Grant No. 12174251), the Natural Science Foundation of Shanghai (Grant No. 22ZR142830), and the Shanghai Municipal Science and Technology Major Project (Grant No. 2019SHZDZX01).

- 
- [1] J. J. Hopfield, *Proc. Natl. Acad. Sci. USA* **79**, 2554 (1982).
  - [2] D. J. Amit, H. Gutfreund, and H. Sompolinsky, *Phys. Rev. Lett.* **55**, 1530 (1985).
  - [3] D. J. Amit, H. Gutfreund, and H. Sompolinsky, *Phys. Rev. A* **32**, 1007 (1985).
  - [4] M. Mezard, G. Parisi, and M. Virasoro, *Spin Glass Theory and Beyond: An Introduction to the Replica Method and Its Applications* (World Scientific, Singapore, 1986).
  - [5] J. L. van Hemmen, *Phys. Rev. Lett.* **49**, 409 (1982).
  - [6] S. F. Edwards and P. W. Anderson, *J. Phys. F: Met. Phys.* **5**, 965 (1975).
  - [7] D. Sherrington and S. Kirkpatrick, *Phys. Rev. Lett.* **35**, 1792 (1975).
  - [8] C. L. Baldwin, C. R. Laumann, A. Pal, and A. Scardicchio, *Phys. Rev. Lett.* **118**, 127201 (2017).
  - [9] S. Mukherjee, S. Nag, and A. Garg, *Phys. Rev. B* **97**, 144202 (2018).
  - [10] L. Rademaker and D. A. Abanin, *Phys. Rev. Lett.* **125**, 260405 (2020).
  - [11] S. J. Thomson, P. Urbani, and M. Schiró, *Phys. Rev. Lett.* **125**, 120602 (2020).
  - [12] M. Winer, R. Barney, C. L. Baldwin, V. Galitski, and B. Swingle, *J. High Energy Phys.* **09** (2022) 32
  - [13] P. Rotondo, M. Marcuzzi, J. Garrahan, I. Lesanovsky, and M. Muller, *J. Phys. A: Math. Theor.* **51**, 115301 (2018).
  - [14] F. Carollo and I. Lesanovsky, *Phys. Rev. Lett.* **126**, 230601 (2021).

- [15] M. Shcherbina, B. Tirozzi, and C. Tassi, *Physics* **2**, 184 (2020).
- [16] D. C. Mattis, *Phys. Lett. A* **56**, 421 (1976).
- [17] H. J. Lipkin, N. Meshkov, and A. J. Glick, *Nucl. Phys.* **62**, 188 (1965).
- [18] J. A. Kjäll, J. H. Bardarson, and F. Pollmann, *Phys. Rev. Lett.* **113**, 107204 (2014).
- [19] V. Oganesyan and D. A. Huse, *Phys. Rev. B* **75**, 155111 (2007).
- [20] E. P. Wigner, *Ann. Math.* **62**, 548 (1955).
- [21] D. A. Huse, R. Nandkishore, V. Oganesyan, A. Pal, and S. L. Sondhi, *Phys. Rev. B* **88**, 014206 (2013).
- [22] L. F. Santos and M. Rigol, *Phys. Rev. E* **81**, 036206 (2010).
- [23] T. N. Ikeda, Y. Watanabe, and M. Ueda, *Phys. Rev. E* **87**, 012125 (2013).
- [24] W. Beugeling, R. Moessner, and M. Haque, *Phys. Rev. E* **89**, 042112 (2014).
- [25] T. Yoshizawa, E. Iyoda, and T. Sagawa, *Phys. Rev. Lett.* **120**, 200604 (2018).
- [26] A. Yoshinaga, H. Hakoshima, T. Imoto, Y. Matsuzaki, and R. Hamazaki, *Phys. Rev. Lett.* **129**, 090602 (2022).
- [27] J. M. Deutsch, *Phys. Rev. A* **43**, 2046 (1991).
- [28] M. Srednicki, *Phys. Rev. E* **50**, 888 (1994).
- [29] L. D'Alessio, Y. Kafri, A. Polkovnikov, and M. Rigol, *Adv. Phys.* **65**, 239 (2016).
- [30] D. M. Basko, I. L. Aleiner, and B. L. Altshuler, *Ann. Phys. (Amsterdam)* **321**, 1126 (2006).
- [31] M. Žnidarič, T. Prosen, and P. Prelovšek, *Phys. Rev. B* **77**, 064426 (2008).
- [32] A. Pal and D. A. Huse, *Phys. Rev. B* **82**, 174411 (2010).
- [33] M. Rigol, V. Dunjko, and M. Olshanii, *Nature (London)* **452**, 854 (2008).
- [34] T. Mori, T. N. Ikeda, E. Kaminishi, and M. Ueda, *J. Phys. B: At., Mol. Opt. Phys.* **51**, 112001 (2018).
- [35] C. J. Turner, A. A. Michailidis, D. A. Abanin, M. Serbyn, and Z. Papić, *Nat. Phys.* **14**, 745 (2018).
- [36] E. A. Yuzbashyan, O. Tsypliyatyev, and B. L. Altshuler, *Phys. Rev. Lett.* **96**, 097005 (2006).
- [37] R. A. Barankov and L. S. Levitov, *Phys. Rev. Lett.* **96**, 230403 (2006).
- [38] Y. Chen and Z. Cai, *Phys. Rev. A* **101**, 023611 (2020).
- [39] K. Sacha, *Phys. Rev. A* **91**, 033617 (2015).
- [40] D. V. Else, B. Bauer, and C. Nayak, *Phys. Rev. Lett.* **117**, 090402 (2016).
- [41] V. Khemani, A. Lazarides, R. Moessner, and S. L. Sondhi, *Phys. Rev. Lett.* **116**, 250401 (2016).
- [42] N. Y. Yao, A. C. Potter, I.-D. Potirniche, and A. Vishwanath, *Phys. Rev. Lett.* **118**, 030401 (2017).
- [43] E. Fiorelli, M. Marcuzzi, P. Rotondo, F. Carollo, and I. Lesanovsky, *Phys. Rev. Lett.* **125**, 070604 (2020).